University of Dayton
eCommons

Chemical and Materials Engineering Faculty Publications | Department of Chemical and Materials Engineering

2015

Effects of Disorder State and Interfacial Layer on Thermal Transport in Copper/Diamond System

Vikas Sinha
Air Force Research Laboratory

Jaime J. Gengler
Air Force Research Laboratory

Christopher Muratore
University of Dayton, cmuratore1@udayton.edu

Jonathan E. Spowart
Air Force Research Laboratory

Follow this and additional works at: https://ecommons.udayton.edu/cme_fac_pub

Part of the Other Chemical Engineering Commons, Other Materials Science and Engineering Commons, and the Polymer and Organic Materials Commons

eCommons Citation

Sinha, Vikas; Gengler, Jaime J.; Muratore, Christopher; and Spowart, Jonathan E., "Effects of Disorder State and Interfacial Layer on Thermal Transport in Copper/Diamond System" (2015). *Chemical and Materials Engineering Faculty Publications*. 97.
https://ecommons.udayton.edu/cme_fac_pub/97

This Article is brought to you for free and open access by the Department of Chemical and Materials Engineering at eCommons. It has been accepted for inclusion in Chemical and Materials Engineering Faculty Publications by an authorized administrator of eCommons. For more information, please contact frice1@udayton.edu, mschlangen1@udayton.edu.

JOURNAL OF APPLIED PHYSICS 117, 074305 (2015)

Effects of disorder state and interfacial layer on thermal transport in copper/diamond system

V. Sinha,[1,2,a)] J. J. Gengler,[1,3] C. Muratore,[1,4] and J. E. Spowart[1]
[1]*Air Force Research Laboratory, Materials and Manufacturing Directorate, Wright-Patterson Air Force Base, Ohio 45433, USA*
[2]*UES, Inc., 4401 Dayton-Xenia Road, Dayton, Ohio 45432, USA*
[3]*Spectral Energies, LLC, 5100 Springfield Street, Suite 301, Dayton, Ohio 45431, USA*
[4]*University of Dayton Research Institute, 300 College Park, Dayton, Ohio 45469, USA*

(Received 18 August 2014; accepted 17 January 2015; published online 19 February 2015)

The characterization of Cu/diamond interface thermal conductance (h_c) along with an improved understanding of factors affecting it are becoming increasingly important, as Cu-diamond composites are being considered for electronic packaging applications. In this study, ~90 nm thick Cu layers were deposited on synthetic and natural single crystal diamond substrates. In several specimens, a Ti-interface layer of thickness ≤3.5 nm was sputtered between the diamond substrate and the Cu top layer. The h_c across Cu/diamond interfaces for specimens with and without a Ti-interface layer was determined using time-domain thermoreflectance. The h_c is ~2× higher for similar interfacial layers on synthetic versus natural diamond substrate. The nitrogen concentration of synthetic diamond substrate is four orders of magnitude lower than natural diamond. The difference in nitrogen concentration can lead to variations in disorder state, with a higher nitrogen content resulting in a higher level of disorder. This difference in disorder state potentially can explain the variations in h_c. Furthermore, h_c was observed to increase with an increase of Ti-interface layer thickness. This was attributed to an increased adhesion of Cu top layer with increasing Ti-interface layer thickness, as observed qualitatively in the current study.
[http://dx.doi.org/10.1063/1.4906958]

I. INTRODUCTION

For reliable operation of high power density electronic devices, an efficient heat removal from hot regions is required. The high thermal conductivity (λ) and low coefficient of thermal expansion of Cu-diamond composites make them preferred materials for these heat sink applications. Consequently, this composite system has been the subject of extensive investigation in recent years.[1–4] Maximization of the metal/diamond interface thermal conductance (h_c) is a promising path to improve the composite λ.[3,5] Therefore, examinations of h_c for Cu/diamond interface and factors influencing it are both of scientific interest and practical importance.

In the absence of an interface layer between Cu and diamond, h_c for Cu/diamond interfaces are quite low and this causes λ of composites also to be very low. For example, Schubert *et al.*[4] reported $\lambda = 215$ W/m-K for a Cu-42 vol. % diamond composite with no interfacial layer. In this case, λ for the composite is significantly lower than for Cu (~400 W/m-K). Thus, in this example, the addition of diamond in Cu matrix leads to a deterioration of the ability to spread heat rather than the desired improvement. For this particular composite, h_c was calculated to be 0.5 MW/m^2-K and this low value of h_c resulted in the low λ.[4] The introduction of a thin interfacial carbide (e.g., Cr_3C_2, B_4C, TiC, etc.) layer between Cu and diamond has been shown to increase the λ of Cu-diamond composites to values well above that of Cu, which is effected due to the improvement in h_c.[2–4,6–8] It has also been established that h_c is inversely related to the thickness of interfacial carbide layer.[3] The calculation of h_c in prior studies[3,4,6,7,9] invoked Hasselman-Johnson[10] and/or differential effective medium[9] models, which requires the composite λ to be one of the input parameters.

There is an alternate method, time-domain thermoreflectance (TDTR),[11–15] to determine h_c for metal/diamond interfaces, which allows precise and more direct measurement for an individual interface rather than an average over a bulk sample. The sample for TDTR examination can be prepared by deposition of thin metallic layers (~90 nm thick) on a diamond substrate. The metal layers are locally heated (temperature increase is ≤1 K) with a pump laser beam, and the change in its reflectance with time and temperature is monitored with a probe laser beam. The modeling of changes in reflectance of metal top layers leads to the determination of h_c. Several studies have employed TDTR or similar techniques to determine h_c for metal/diamond interfaces.[16–18] Recent advances with two-color[13,18,19] TDTR have greatly improved the characterization of specimens with a Cu top layer. Gengler *et al.*[19] reported an $h_c \sim 60$ MW/m^2-K for an interface between Cu and highly oriented pyrolitic graphite (HOPG), whereas Monachon and Weber[18] reported an $h_c \sim 35$ MW/m^2-K for an interface between Cu and diamond. There are no prior reports on TDTR-determined h_c for a material system, where an interface layer is introduced between Cu and diamond.

In the current research, a Ti interface layer is introduced between Cu and diamond, and the h_c for this material system is determined with TDTR. The objective of this study is to determine if the presence of a Ti interface layer improves the

a)Author to whom correspondence should be addressed. Electronic mail: vikas.sinha.1.ctr@us.af.mil

h_c, akin to an enhancement effected by carbide interface layers in the case of Cu-diamond composites. Furthermore, the thickness of Ti interface layer is systematically varied and the h_c is determined using TDTR for different Ti layer thicknesses. This part of the study was aimed at identifying any correlations between h_c and the Ti interface layer thickness. Stoner and Maris[16] have used molecular-dynamics (MD) simulations to demonstrate that the strength of the potential binding metal to the substrate has a significant effect on the predicted h_c, with a higher strength resulting in a higher h_c. Transition metals such as Ti and Cr bond strongly to carbon and, moreover, Ti has a stronger bond with carbon than Cr.[20] Furthermore, it has been shown experimentally that another carbon-based material has a higher h_c with Ti than with Cr,[19,20] despite a better matching of vibrational density of states with Cr than with Ti. Therefore, Ti was selected as the interface layer between Cu and diamond in the current study.

In their seminal paper,[21] Swartz and Pohl concluded that bulk disorder near the interface can cause significant deviations in the experimentally determined h_c from its model prediction. In the current study, the concentrations of nitrogen and other impurities (e.g., hydrogen, oxygen, etc.) were measured as these may contribute to the disorder. Secondary ion mass spectrometry (SIMS) was used for concentration measurements as a function of depth below the sample surface. Atomic force microscopy (AFM) was used to measure the surface roughness of diamond substrates. The differences in h_c of specimens with synthetic and natural diamond substrates are discussed in the context of variations in near-surface disorder and interface roughness.

II. EXPERIMENTAL PROCEDURES

In this study, two different types of single crystal diamond substrates, synthetic and natural, were used to make specimens for h_c determinations. The synthetic and natural diamond substrates were supplied by Element Six (Santa Clara, CA) and Blue Nile (Seattle, WA), respectively. Their crystallographic orientations were determined with electron backscattered diffraction (EBSD) techniques in an FEI XL-30 scanning electron microscope (SEM) with a field emission gun (FEG). The diamond substrates were tilted at 70° in the SEM sample chamber, and the EBSD patterns were acquired with TSL OIM Data Collection software (supplier: TexSEM Laboratories, Inc., Draper, UT, USA) at an accelerating voltage of 20 kV and a working distance of 25 mm. Several Kikuchi bands in each EBSD pattern were detected manually and indexing of the pattern yields the crystallographic orientation of diamond substrates. The manual detection method has been used previously to determine the crystallographic orientation of fracture facets in Ti-alloys.[22,23] The EBSD technique of crystallographic orientation determination is known to be accurate within $\pm 1°$.[24] The crystallographic orientations of diamond substrates were depicted in inverse pole figures using TSL OIM Analysis software.

The SIMS experiments were carried out in a Cameca IMS 4F unit with Cs^+ as the primary ion beam at 14.5 keV. The concentrations of six elements (nitrogen, hydrogen, oxygen, fluorine, chlorine, and sulfur) as a function of depth were measured in both the synthetic and natural diamond substrates. CN^-, H^-, O^-, F^-, Cl^-, and S^- secondary ions were monitored for concentration quantification of N, H, O, F, Cl, and S, respectively. To minimize the contributions of $^{13}C_2^-$ to CN^- counts, high mass resolution spectrum was utilized in the case of CN^- secondary ions. The conversion of the measured secondary ion counts to concentration was accomplished using relative sensitivity factors from carbon standards. The depth scale was calibrated by measuring the depth of analysis crater with a stylus profilometer. The detection limits for the different elements are shown in Table I.

The roughness was measured *via* AFM in a Bruker Nanoscope. The scan size was $30\,\mu m \times 30\,\mu m$, the scan rate was 1 Hz, and the measurements were conducted in the tapping mode.

The metal films were deposited on the diamond substrates via magnetron sputtering. A direct current (DC) process was used for deposition of the Cu top layer; whereas a high power pulsed magnetron sputtering process was used for deposition of the Ti-interface layer. The high power pulsed process differs from ordinary sputtering in that (1) the metal flux is composed primarily of ions rather than neutrals and (2) the maximum kinetic energy of the incident ions is significantly larger ($\sim$10–15 eV) than in ordinary sputtering. The base pressure for magnetron sputtering apparatus was less than 5×10^{-9} Torr, and the pure metal (Ti and Cu) targets were sputtered in 10 mTorr of ultra-high purity Ar. The maximum temperature of the substrate surface during deposition was approximately 70 °C as measured by a calibrated infrared pyrometer aimed at the sample surface.

The sputter-coated diamond substrates were characterized with electron probe microanalysis (EPMA) to determine the thickness of metallic film(s). The EPMA experiments were conducted using Cameca SX100 unit operating at 15 kV. Data from EPMA experiments were modeled to determine the metal layer thickness. Several software packages (e.g., GMRFILM, Strata, and Multifilm) have been developed by different research groups to process the EPMA data for determinations of film thickness and composition.[25–27] GMRFILM permits the determination of film thickness (with an accuracy of $\pm$10%) from experimentally determined X-ray intensity ratios (*k*-ratios) and known film density, as described in Ref. 25. In the current work, the *k*-ratios for the elements of interest (i.e., Cu and Ti) were determined with EPMA experiments using wavelength-dispersive spectrometer (WDS) on the surface Cu-film on diamond

TABLE I. Detection limits of analyzed elements in diamond.

Element	Detection limit (atoms/cm^3)
H	2×10^{17}
N	2×10^{15}
O	5×10^{16}
F	5×10^{14}
S	1×10^{15}
Cl	1×10^{15}

substrates and on pure elemental (Cu and Ti) standards. The k-ratios and density of metals ($\rho_{Cu} = 8.89 \times 10^3\,kg/m^3$ and $\rho_{Ti} = 4.51 \times 10^3\,kg/m^3$) were entered in the GMRFILM program to calculate the metallic layer thicknesses. Prior studies report a good correlation of thin film thickness values determined using EPMA with those determined using Transmission Electron Microscopy (TEM),[25] Spectroscopic Ellipsometry,[25] and Rutherford Backscattering Spectrometry (RBS).[25,27] The experiments in our laboratory on sputter-coated metal films also confirmed a good correlation of thin film thickness values determined using EPMA–GMRFILM method with those determined using TEM, Profilometry, and RBS. Therefore, EPMA–GMRFILM technique is expected to provide accurate values of metallic layer thicknesses in the current research.

Thermal conductance of the Cu/diamond interfaces was determined with a two-color TDTR lab.[13] The output of a mode-locked Ti:sapphire laser is split into a pump and a probe beam. The pump beam (wavelength ~785 nm) is sent first through a pulse compressor and then through an electro-optic modulator (EOM), which imposes a square-wave pulse train with a frequency of 9.8 MHz. The pump beam is then aligned along a mechanical translation stage to systematically alter the timing between the pump and the probe pulses. The probe beam is sent through an optical parametric oscillator (OPO) to modify its wavelength to ~600 nm. Both beams are then focused to a spot size of ~50 μm at a 45° angle to the sample. The reflected probe beam is spatially filtered, recollimated, and sent through a 750 nm short pass optical filter to reject scattered pump-beam light. Finally, the probe beam is passed through a neutral-density filter (optical density = 1.0) and focused onto a silicon photodiode detector. The output of the detector is sent to the input of a dual phase, radio frequency lock-in amplifier that has its reference channel connected to the same electronic signal that drives the EOM. The scans and data acquisition are computer controlled with a LABVIEW program developed in our laboratory. TDTR data were acquired from five randomly chosen locations on each sample surface. Data analysis was performed with a nonlinear least squares application to Cahill's frequency domain model[14] to determine h_c for Cu/diamond interfaces. The results from the five scans on each sample were used to establish an average ± standard deviation value. Although specimens had up to 3.5 nm thick (as described below in Sec. III) Ti-interface layer between Cu and diamond, the modeling of TDTR data is reported to provide h_c for Cu/diamond interface, as the conduction across Ti-layer was not modeled separately. This approach is similar to that reported in Ref. 15, where 3 nm thick Ti adhesion layer was inserted between Cu and sapphire, and the modeling of TDTR data was reported to provide h_c for Cu/sapphire interface.

III. RESULTS

The EBSD patterns for the synthetic and natural diamond substrates are shown in Figures 1(a) and 1(d), respectively. The patterns at different locations throughout the top

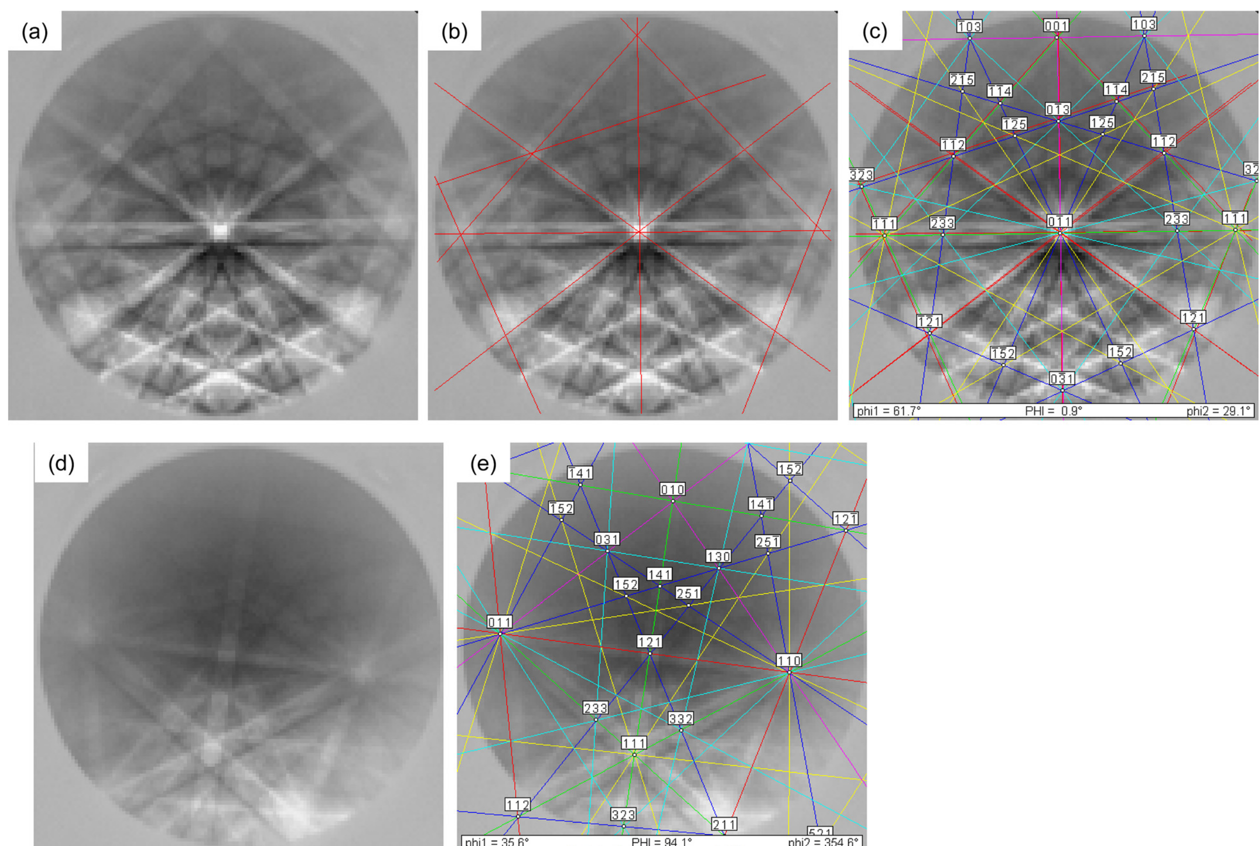

FIG. 1. Determination of crystallographic orientation of diamond substrates with EBSD technique in an SEM. (a) EBSD pattern from synthetic (CVD) diamond, (b) manual detection of Kikuchi bands in pattern (a), (c) indexing of pattern (a), (d) EBSD pattern from natural diamond, and (e) indexing of pattern (d).

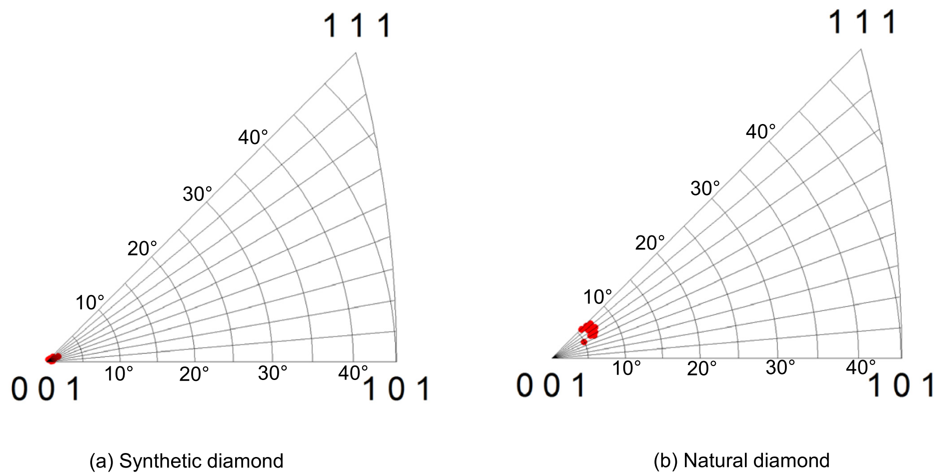

FIG. 2. Inverse pole figures showing the crystallographic orientation of diamond substrates. The red closed circles depict the orientation of surface normal in the stereographic triangle for diamond crystal, which were determined with EBSD at 13 different locations on the substrate. (a) Synthetic diamond and (b) natural diamond.

polished surface of each substrate remained essentially unchanged, which confirms that the substrates are single crystals. Several of the Kikuchi bands are detected manually and are shown as red lines in Figure 1(b). The indexed patterns for synthetic and natural diamond substrates are shown in Figures 1(c) and 1(e), respectively. The crystallographic orientations of diamond substrates are shown in Figure 2.

The SIMS depth profiles for the synthetic and natural diamond substrates are shown in Figures 3 and 4. The bulk nitrogen concentration of synthetic diamond substrate is 2.2×10^{16} atoms/cm^3 (i.e., 0.15 ppm by weight), which is approximately four orders of magnitude smaller than the value of 1.33×10^{20} atoms/cm^3 (i.e., 883 ppm by weight) for natural diamond substrate. The bulk concentrations of hydrogen, oxygen, sulfur, chlorine, and fluorine in both the diamond substrates are below the detection limit for the element of interest (Figure 4 and Table I).

The surface profiles for the two substrates are shown in Figure 5. The roughness of synthetic diamond is higher than the natural diamond. The root mean squared roughness (R_q) values for synthetic and natural diamonds are 5.8 and 2.8 nm, respectively. The average roughness (R_a) values for synthetic and natural diamonds are 2.3 and 1.6 nm, respectively. Furthermore, the surface topography is more uniform for natural diamond than synthetic diamond (Figure 5).

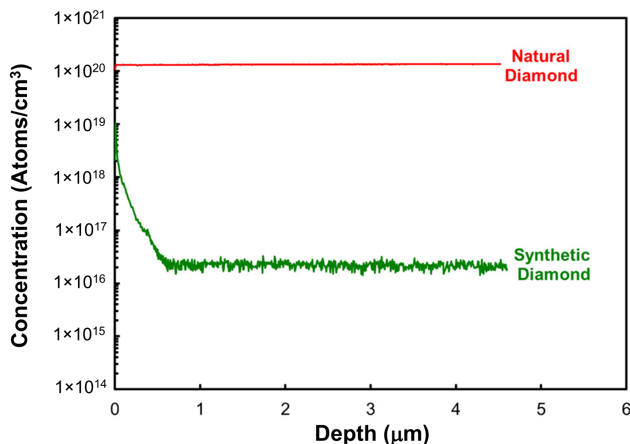

FIG. 3. SIMS depth profiles showing nitrogen concentration as a function of depth below the surface for synthetic and natural diamond substrates.

The thickness of Ti-interface layer ranged between 0 and 3.5 nm on different specimens, as determined with GMRFILM modeling of data acquired via EPMA. The thickness of the Cu top layer was also determined with GMRFILM modeling of EPMA data, and it varied in the range of 73–133 nm for different specimens.

The h_c values determined via TDTR method are depicted in Figure 6 for the two types of diamond substrates (synthetic and natural) and for a range of thicknesses of the Ti-interface layer. Each of the data points in Figure 6 is an average of measurements at five different locations on a specimen, whereas the error bars indicate standard deviation for each set of five measurements. Two specimens with the synthetic diamond substrate and without any Ti-interface layer were prepared, and characterized with TDTR. The h_c values for these two specimens are shown as two different data points in Figure 6, and demonstrate that the reproducibility of methodology, including specimen preparation and TDTR characterization, employed in the current study is within $\pm 10\%$.

Our results are compared with the predictions of the acoustic mismatch model (AMM) that assumes no phonon scattering at the interface, and the diffuse mismatch model (DMM) that assumes scattering of all phonons incident on the interface.[21] According to AMM, the Cu/diamond interface thermal conductance is given by[28,29]

$$h_c \approx \frac{1}{2}\rho_m.c_{p_m}.\frac{v_m^3}{v_d^2}.\frac{\rho_m\rho_d v_m v_d}{(\rho_m v_m + \rho_d v_d)^2}\ , \tag{1}$$

where ρ_m and ρ_d are the densities of Cu and diamond, respectively, v_m and v_d are the phonon velocities in Cu and diamond, respectively, and c_{p_m} is the specific heat capacity of Cu. Using $\rho_m = 8960$ kg/m^3, $c_{p_m} = 385$ J/kg-K, $v_m = 2881$ m/s, $\rho_d = 3520$ kg/m^3, and $v_d = 13\,924$ m/s as input parameters[28] in Eq. (1), h_c for Cu/diamond interface is estimated to be 48.1 MW/m^{2}K^3. This AMM-predicted value of h_c is shown as a dashed horizontal line in Figure 6.

DMM assumes that all the phonons are randomly and elastically scattered at the interface, and the scattering probability into each material is decided by the density of phonon states in each material.[21,30] The transmission probability is written as

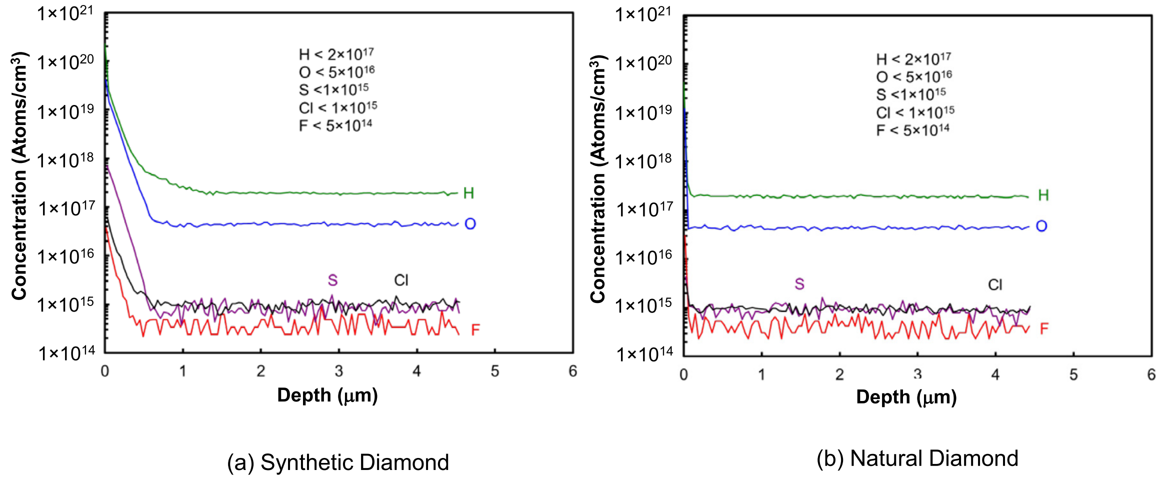

FIG. 4. SIMS depth profiles showing concentrations of hydrogen, oxygen, sulfur, chlorine, and fluorine as a function of depth below the surface for (a) synthetic and (b) natural diamond substrates.

$$\alpha_{1,j}(\omega) = \frac{v_{2,j}\, g_{2,j}(\omega)}{v_{1,j}\, g_{1,j}(\omega) + v_{2,j}\, g_{2,j}(\omega)} , \tag{2}$$

where $\alpha_{i,j}(\omega)$ is the phonon transmission probability of mode j on side i, ω is the phonon angular frequency, $v_{i,j}$ is the phonon sound velocity of mode j on side i, and $g_{i,j}(\omega)$ is the density of phonon states of mode j on side i. The interface thermal conductance is given by[21,30]

$$h_c = \frac{1}{2}\sum_{i,j}\frac{\partial}{\partial T}\int_0^{\pi/2}\int_0^{\omega_i^{max}} \alpha_{i,j}(\theta,\omega,j) g_{i,j}(\omega) n(\omega,T)\hbar\omega v_{i,j} \times \cos\theta \sin\theta\, d\theta\, d\omega, \tag{3}$$

where θ is the phonon incident angle, ω_i^{max} is the maximum phonon angular frequency on side i, $\hbar$ is Planck's constant divided by 2π, and $n(\omega,T)$ is the Bose occupation distribution function. $n(\omega,T)$ is given by[30]

$$n(\omega,T) = \frac{1}{e^{\hbar\omega/k_B T} - 1} , \tag{4}$$

where k_B is Boltzmann's constant and T is the temperature.

From the DMM, the h_c for Cu/diamond interface was calculated to be 88.6 MW/m^2K.[30,31] This DMM-predicted value of h_c is also shown in Figure 6 as another dashed horizontal line.

For a qualitative assessment of the adhesion of Cu film on diamond for specimens with different thickness of Ti-interface layer, it was attempted to remove the metal film from diamond substrates using Scotch® tape. It was observed that insertion of Ti-interface layer improves the adhesion of Cu to diamond, as it was more difficult to remove the Cu film. Furthermore, the Cu top layer adhered more strongly to diamond with an increase of Ti-interface layer thickness. These results provide an idea about the variation in Cu film adherence to diamond substrate, albeit qualitatively, with change in the Ti-interface layer thickness.

IV. DISCUSSION

The h_c of specimens with synthetic diamond substrate is higher than with natural diamond substrate (Figure 6). It is clear from Figure 2 that the surface of both the diamond substrates is parallel to the (001) crystallographic plane. Thus, the crystallography of surface is essentially the same for two

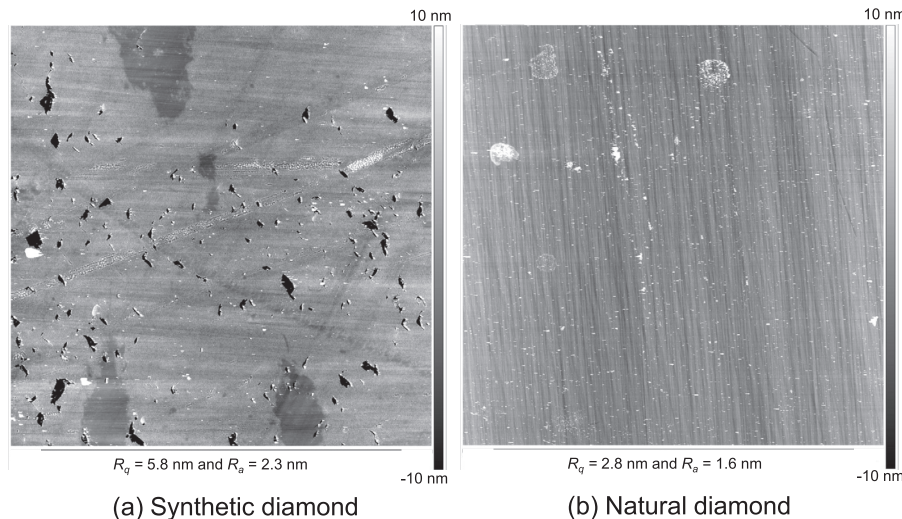

FIG. 5. Surface profiles (scan area $= 30\,\mu m \times 30\,\mu m$) acquired with AFM. (a) Synthetic and (b) natural diamond substrates. R_q and R_a denote root mean squared and average roughness, respectively.

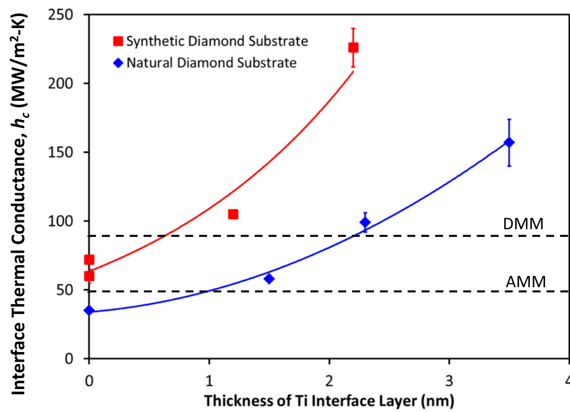

FIG. 6. Effect of Ti interface layer thickness on Cu/diamond interface thermal conductance. The solid lines depict the approximate trend for experimental data points. The dashed horizontal lines depict the predictions of AMM and DMM for Cu/diamond interface.

types of diamond substrates. The substantially lower nitrogen concentration in synthetic diamond than in natural diamond (Figure 3) and essentially similar bulk concentrations of H, O, S, Cl, and F in the two diamonds (Figure 4) suggest that the degree of disorder in synthetic diamond is significantly less than in the natural diamond substrate. Since λ of diamond is known to decrease with an increase of its nitrogen content,[32] this also implies that synthetic diamond has a higher λ. This is further supported by the modeling of TDTR data, which suggests that λ of synthetic diamond is higher than natural diamond. In this context, it is interesting to note that Swartz and Pohl have suggested that bulk disorder in the near-surface region can potentially cause significant variations in h_c and therefore, an improved understanding of this disorder is highly desirable.[21] The current study provides the experimental evidence of variations in nitrogen concentration of the natural and synthetic diamond substrates, which can lead to variations in the degree of bulk disorder in near-surface regions of the two substrates. This can explain, at least in part, the differences in h_c of specimens with natural and synthetic diamond substrates. In addition to the differences in nitrogen concentration, the roughness and uniformity of surface topography for the two substrates are different. In this discussion, it is relevant that Hopkins *et al.* have reported a reduction in h_c for Al/Si interfaces with an increase of substrate surface roughness.[33] Assuming a similar relationship between substrate surface roughness and h_c for Cu/diamond interfaces, the h_c for specimens with synthetic diamond substrate is expected to be lower than with natural diamond substrate, which is opposite of the observed behavior (Figure 6). There are two possible reasons for this apparent deviation from expected behavior: (a) difference in average surface roughness is small (2.3 nm for synthetic diamond versus 1.6 nm for natural diamond), which can result in only small variations in h_c and (b) there is a significant difference in nitrogen concentration (four orders of magnitude lower in synthetic than in natural diamond), which can more than compensate for any small variations in h_c due to differences in surface roughness and topography.

The values of h_c of specimens with synthetic and natural diamond substrates are compared with the predictions of AMM and DMM (Figure 6). The h_c of specimens with synthetic diamond substrate (without Ti-interface layer) lies in between the AMM and DMM-predicted values. This is consistent with Ref. 21, where the experimental measurements of Kapitza resistance for Cu/helium by different researchers were reported to lie in between the predictions of AMM and DMM. The h_c of specimen with natural diamond substrate (without Ti-interface layer) is lower than even the AMM-predicted value (Figure 6), which presumably is due to a significantly higher level of bulk disorder in this substrate.

For specimens with either synthetic or natural diamond substrate, the presence of Ti-interface layer causes an increase in h_c, when compared with the specimens without any interface layer (Figure 6). This can be explained by a higher interfacial bond strength between Ti and diamond than between Cu and diamond. Both the simulations by Stoner and Maris[16] and the experimental work of Collins *et al.*[17] suggest that the strength of interfacial bonding may have a strong influence on h_c, which can help rationalize the findings of current research.

For specimens with either synthetic or natural diamond substrate, an increase in Ti-interface layer thickness clearly results in an increase in h_c (Figure 6). A consideration of the relative values of the mean free path (MFP) of heat carriers (i.e., electrons) in bulk Ti and the Ti-interface layer thickness, in the context of Fuchs-Sondheimer size-effect theory,[34,35] suggests that the λ of interfacial Ti-layer would increase with an increase in its thickness. The bulk MFP (Λ_b) of conduction electrons in Ti at room temperature is 28.5 nm,[36] which is at least 8× longer than the Ti-interface layer thicknesses examined in current study. In addition to the scattering mechanisms operational in bulk Ti, the electrons in thin Ti-interface layers are also expected to scatter at Cu/Ti and Ti/diamond interfaces, which would result in the effective MFP (Λ_{eff}) of electrons in Ti-interface layer to be significantly less than Λ_b. The distributions of Λ_b and film MFP (Λ_f) are shown schematically in Figure 7. Λ_{eff} can be calculated using equation:[37] $\Lambda_{eff}^{-1} = \Lambda_b^{-1} + \Lambda_f^{-1}$. For the current case of Ti-interface layer thickness being significantly less than Λ_b, an increase in Ti-layer thickness causes an increase in Λ_f and thereby in Λ_{eff}, which in turn causes an increase in λ of interfacial Ti-layer. According to Fuchs-Sondheimer size-effect theory,[35] for $\kappa \ll 1$

$$\frac{\lambda_f}{\lambda} = \frac{3}{4} \times \frac{(1+p)}{(1-p)} \times \kappa \ln\left(\frac{1}{\kappa}\right), \tag{5}$$

where λ_f is the thermal conductivity of Ti film, λ (=21.9 W/m-K) is the thermal conductivity of bulk Ti, p is assumed to be the fraction of elastically scattered electrons (the remainder are scattered diffusely at the interface), and $\kappa = \frac{\text{film thickness}}{\Lambda_b}$. λ_f is calculated for the range of interface layer thicknesses examined in current study and its variation with interface layer thickness is shown in Figure 8(a). Two values of p (= 0 and 0.5) are considered. λ_f increases with an increase of interface layer thickness (the rate of increase is higher at the higher p of 0.5). This could be a possible reason for observed increase in h_c with Ti interface layer thickness (Figure 6). To check this possibility further, h_c for the Ti

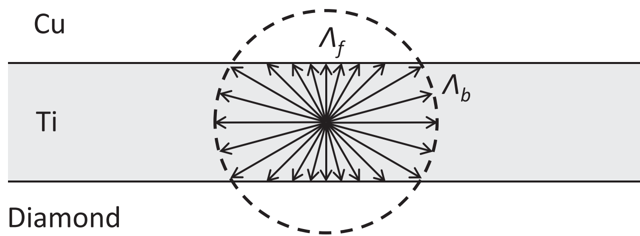

FIG. 7. Electron mean free path distribution in Ti interface layer (schematic). Bulk MFP (Λ_b) is determined by the scatterings with phonons and impurities, whereas film MFP (Λ_f) is determined by the scatterings at Ti/Cu and Ti/diamond interfaces. Λ_f is shorter than Λ_b (After Ref. 37).

interface layer was calculated as: $h_c = \frac{\lambda_f}{\text{film thickness}}$ (as discussed, for example, in Ref. 7). Figure 8(b) shows that h_c of Ti interface layer actually *decrease*s with an increase of its thickness even though λ_f increases, and this drop in h_c is more significant for a higher p. It appears that the increase in Ti-layer thickness more than compensates the increase in its λ_f, which results in the h_c of Ti interface layer to decrease. Second, a comparison of Figures 6 and 8(b) suggests that h_c of Ti interface layer is an order of magnitude higher than the h_c for specimens examined in the current study. Therefore, it is concluded that Fuchs-Sondheimer size-effect theory cannot explain the observed variation in h_c with Ti interface layer thickness, which is depicted in Figure 6.

As discussed in Sec. III, the Cu top layer adhered more strongly to diamond with an increase of Ti-interface layer thickness. In this context, it is interesting to note that a modified acoustic mismatch model proposed by Prasher[38] predicts that h_c is proportional to the square of adhesion energy of the interface for the case of weak bonding. Therefore, the increase in h_c with increasing Ti interface layer thickness is attributed to an improvement in metal layer adherence and the resultant increase in interfacial adhesion energy.

Schmidt *et al.*[20] reported that the values of h_c for a Ti/c-axis oriented HOPG specimen and an Al/c-axis oriented HOPG specimen with a 5 nm thick Ti-adhesion (interface) layer between Al and HOPG were similar. By analogy, it is expected that the h_c for a Cu/diamond specimen with a 3.5 nm thick Ti-interface layer in the current study will be similar to a Ti/diamond specimen. Stoner and Maris[16] measured an $h_c = 100$ MW/m^2-K for Ti/diamond specimen at room temperature, which is lower than 157 MW/m^2-K measured in the current study for a Cu/diamond specimen with 3.5 nm thick Ti-interface layer. This difference could be associated with possible differences in the disorder state of the diamond substrates in the two studies, as was observed for the specimens with synthetic and natural diamond substrates in the current study. Furthermore, the lattice dynamical calculations in the same study predict a value of 70 MW/m^2-K for h_c across Ti/diamond interface,[16] which again is lower than the h_c of 157 MW/m^2-K for the Cu/diamond specimen with a 3.5 nm thick Ti-interface layer characterized in the current study. However, the diffuse mismatch limit is higher than the prediction of lattice dynamics modeling, and radiation limit is even higher than the diffuse mismatch limit.[16] It is expected that the diffuse mismatch and radiation limits for Ti/diamond interface will better match the h_c measured in current study for Cu/diamond specimen with a 3.5 nm thick Ti-interface layer.

V. SUMMARY AND CONCLUSIONS

The interface thermal conductance between Cu and diamond was measured using TDTR method. Very thin Ti interface layers ($\leq$3.5 nm thick) were introduced between Cu and diamond, and the effects on h_c of presence of Ti at the interface as well as variation in its thickness were examined. The specimens for TDTR characterization were prepared via magnetron sputtering of metal layers (Cu and Ti) on synthetic and natural single crystal diamond substrates. The results indicate that the values of h_c for specimens with synthetic diamond substrate are $\sim 2\times$ higher than for specimens with natural diamond substrate. This difference can be attributed to a lower level of disorder in near-surface region of synthetic diamond substrate, as a result of significantly lower nitrogen concentration than natural diamond. Furthermore, the presence of a Ti-interface layer increases the h_c in specimens with either synthetic or natural diamond substrate. The h_c is directly related to the Ti-interface layer thickness, within the range

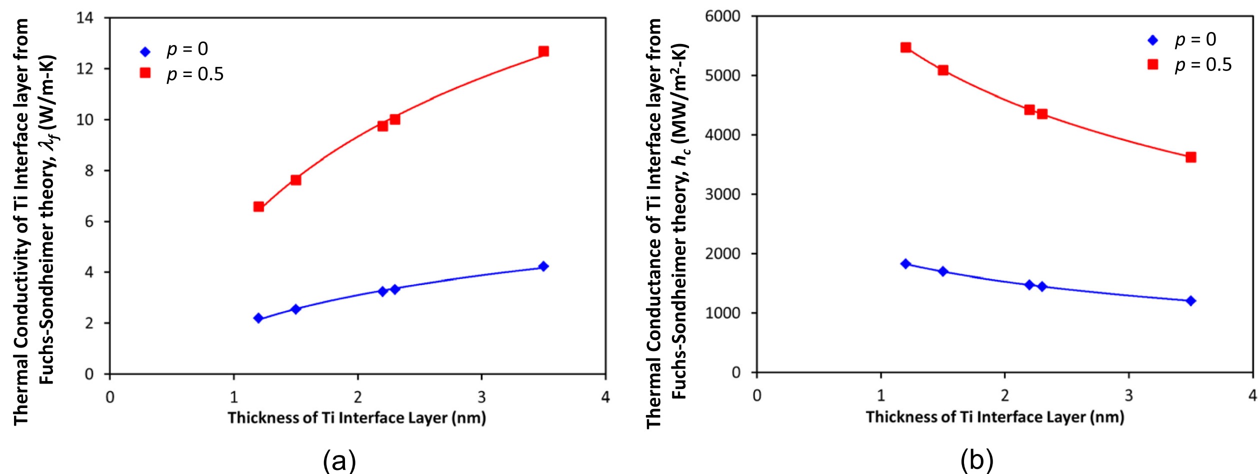

FIG. 8. Calculations using Fuchs-Sondheimer size-effect theory showing the influence of Ti interface layer thickness on its (a) thermal conductivity and (b) thermal conductance. p denotes the fraction of elastically scattered electrons. The solid lines depict the logarithmic fit through the calculated values.

of thicknesses examined in the current study. An enhanced adhesion of Cu top layer with increasing Ti-interface layer thickness causes an increase in h_c.

ACKNOWLEDGMENTS

This research was supported by Air Force Office of Scientific Research under Thermal Sciences Portfolio (Program Manager: Dr. Joan Fuller, LRIR No. 11RX02COR) and performed at Air Force Research Laboratory, Materials and Manufacturing Directorate (Contract Nos. F33615-04-D-5235, FA8650-07-D-5800, and FA8650-10-D-5226). The authors thank Dr. A. A. Voevodin (AFRL) for useful technical discussions and for making the TDTR apparatus available for this study. Dr. F. Meisenkothen (NIST, formerly with UES, Inc.) and Mr. Jared Shank (UES, Inc.) helped with the metal layer thickness measurements via EPMA–GMRFILM Model. We thank Dr. B. M. Howe (AFRL) for help with RBS, Dr. M. E. McConney (AFRL) for help with AFM experiments, and Dr. H. E. Smith (UDRI) for useful discussions on SIMS.

[1]C. Zweben, "High-power diode laser technology and applications II," Proc. SPIE **5336**, 166–175 (2004).
[2]L. Weber and R. Tavangar, Scr. Mater. **57**, 988 (2007).
[3]V. Sinha and J. E. Spowart, J. Mater. Sci. **48**(3), 1330 (2013).
[4]T. Schubert, B. Trindade, T. Weißgärber, and B. Kieback, Mater. Sci. Eng., A **475**, 39 (2008).
[5]R. Tavangar and L. Weber, Emerging Mater. Res. **1**(EMR2), 67 (2012).
[6]T. Schubert, Ł. Ciupiński, W. Zieliński, A. Michalski, T. Weißgärber, and B. Kieback, Scr. Mater. **58**, 263 (2008).
[7]Y. Zhang, H. L. Zhang, J. H. Wu, and X. T. Wang, Scr. Mater. **65**, 1097 (2011).
[8]Ł. Ciupiński, D. Siemiaszko, M. Rosiński, A. Michalski, and K. J. Kurzydłowski, Adv. Mater. Res. **59**, 120 (2009).
[9]R. Tavangar, J. M. Molina, and L. Weber, Scr. Mater. **56**, 357 (2007).
[10]D. P. H. Hasselman and L. F. Johnson, J. Compos. Mater. **21**(6), 508 (1987).
[11]H.-K. Lyeo and D. G. Cahill, Phys. Rev. B **73**, 144301 (2006).
[12]J. J. Gengler, C. Muratore, A. K. Roy, J. Hu, A. A. Voevodin, S. Roy, and J. R. Gord, Compos. Sci. Technol. **70**, 2117 (2010).
[13]J. J. Gengler, S. Roy, J. G. Jones, and J. R. Gord, Meas. Sci. Technol. **23**, 055205 (2012).
[14]D. G. Cahill, Rev. Sci. Instrum. **75**, 5119 (2004).
[15]B. C. Gundrum, D. G. Cahill, and R. S. Averback, Phys. Rev. B **72**, 245426 (2005).
[16]R. J. Stoner and H. J. Maris, Phys. Rev. B **48**, 16373 (1993).
[17]K. C. Collins, S. Chen, and G. Chen, Appl. Phys. Lett. **97**, 083102 (2010).
[18]C. Monachon and L. Weber, Emerging Mater. Res. **1**(EMR2), 89 (2012).
[19]J. J. Gengler, S. V. Shenogin, J. E. Bultman, A. K. Roy, A. A. Voevodin, and C. Muratore, J. Appl. Phys. **112**, 094904 (2012).
[20]A. J. Schmidt, K. C. Collins, A. Minnich, and G. Chen, J. Appl. Phys. **107**, 104907 (2010).
[21]E. T. Swartz and R. O. Pohl, Rev. Mod. Phys. **61**(3), 605 (1989).
[22]V. Sinha, M. J. Mills, and J. C. Williams, J. Mater. Sci. **42**(19), 8334 (2007).
[23]V. Sinha, M. J. Mills, and J. C. Williams, Metall. Mater. Trans. A **37**, 2015 (2006).
[24]M. C. Demirel, B. S. El-Dasher, B. L. Adams, and A. D. Rollett, in *Electron Backscatter Diffraction in Materials Science*, edited by A. J. Schwartz, M. Kumar, and B. L. Adams (Kluwer Academic/Plenum Publishers, New York, NY, USA, 2000), pp. 65–74.
[25]R. A. Waldo, M. C. Militello, and S. W. Gaarenstroom, Surf. Interface Anal. **20**, 111 (1993).
[26]J. L. Pouchou and F. Pichoir, Scanning Microsc. Suppl. **7**, 167 (1993).
[27]J. L. Pouchou, Anal. Chim. Acta **283**, 81 (1993).
[28]K. Chu, Z. Liu, C. Jia, H. Chen, X. Liang, W. Gao, W. Tian, and H. Guo, J. Alloys Compd. **490**, 453 (2010).
[29]K. Chu, C. Jia, X. Liang, H. Chen, W. Gao, and H. Guo, Mater. Des. **30**, 4311 (2009).
[30]H. Wang, Y. Xu, M. Shimono, Y. Tanaka, and M. Yamazaki, Mater. Trans. **48**(9), 2349 (2007).
[31]See http://mits.nims.go.jp/index_en.html for "Interfacial Thermal Conductance Database," NIMS Materials Database (accessed October 14th, 2014).
[32]Y. Yamamoto, Y. Imai, K. Tanabe, T. Tsuno, Y. Kumazawa, and N. Fujimori, Diamond Relat. Mater. **6**, 1057 (1997).
[33]P. E. Hopkins, L. M. Phinney, J. R. Serrano, and T. E. Beechem, Phys. Rev. B **82**, 085307 (2010).
[34]K. Fuchs, Proc. Cambridge Philos. Soc. **34**, 100 (1938).
[35]E. H. Sondheimer, Adv. Phys. **1**, 1 (1952).
[36]B. Singh and N. A. Surplice, Thin Solid Films **10**, 243 (1972).
[37]J. S. Jin, J. S. Lee, and O. Kwon, Appl. Phys. Lett. **92**, 171910 (2008).
[38]R. Prasher, Appl. Phys. Lett. **94**, 041905 (2009).